Actin and Light Chain Isoform Dependence of Myosin V Kinetics†

Enrique M. De La Cruz, Amber L. Wells, H. Lee Sweeney, and E. Michael Ostap*

University of Pennsylvania School of Medicine, Department of Physiology, Pennsylvania Muscle Institute, 3700 Hamilton Walk, Philadelphia, Pennsylvania 19104-6085

Received July 21, 2000; Revised Manuscript Received September 20, 2000

ABSTRACT: Recent studies on myosin V report a number of kinetic differences that may be attributed to the different heavy chain (chicken vs mouse) and light chain (essential light chains vs calmodulin) isoforms used. Understanding the extent to which individual light chain isoforms contribute to the kinetic behavior of myosin V is of critical importance, since it is unclear which light chains are bound to myosin V in cells. In addition, all studies to date have used α-skeletal muscle actin, whereas myosin V is in nonmuscle cells expressing β- and γ-actin. Therefore, we characterized the actin and light chain dependence of single-headed myosin V kinetics. The maximum actin-activated steady-state ATPase rate (V_{max}) of a myosin V construct consisting of the motor domain and first light chain binding domain is the same when either of two essential light chain isoforms or calmodulin is bound. However, with bound calmodulin, the K_{ATPase} is significantly higher and there is a reduction in the rate and equilibrium constants for ATP hydrolysis, indicating that the essential light chain favors formation of the M·ADP·P_i state. No kinetic parameters of myosin V are strongly influenced by the actin isoform. ADP release from the actin−myosin complex is the rate-limiting step in the ATPase cycle with all actin and light chain isoforms. We postulate that although there are significant light-chain-dependent alterations in the kinetics that could affect myosin V processivity in in vitro assays, these differences likely are minimized under physiological conditions.

Myosin V is an unconventional myosin thought to traffic vesicles on actin filaments processively, as a single, two-headed molecule (*1*). Recent reports (*2*−*4*) have detailed the kinetic alterations that enable myosin V to transport cargo along actin filaments at extremely low motor densities. There are disagreements in these reports concerning the rate-limiting step in the actomyosin V ATPase[1] cycle that call into question the predicted degree of processivity that the native, two-headed molecule would display. Some discrepancies may result from technical difficulties associated with measuring the steady-state actin-activated ATPase activity due to a high degree of product (ADP) inhibition of myosin V (*5*). However, the myosin heavy chain (chicken vs mouse) and light chain isoforms (essential light chain LC-1sa vs calmodulin) used could potentially account for some kinetic differences.

The light chain identity is of particular interest, given the previous analysis of the light chain and calmodulin binding sites (IQ motifs) of unconventional myosin family members (*6*, *7*). It has been demonstrated that either an essential light chain or calmodulin can occupy the first IQ motif of myosin V (*2*−*4*), but variations within the IQ motif and sequence differences of the light chains may contribute to the specificity of the interaction (*6*). Tissue purified myosin V shows the presence of at least two light chains in addition to calmodulin, but the identities and binding sites of these light chains (17 and 23 kDa) are not known (*8*).

In this study, we determined the effects of the light chain bound to the first IQ motif on the kinetics of the single-headed myosin V ATPase cycle. Also of note, and of potential physiological importance, is that all of the published studies on myosin V kinetics used skeletal muscle α-actin. Myosin V is enriched in nonmuscle cells and would normally encounter either β- or γ-actin. Thus, we also examined the possible kinetic changes associated with actin isoforms.

MATERIALS AND METHODS

Reagents and Protein Purification. All reagents were of the highest purity commercially available. ATP was purified by anion-exchange chromatography (purity >99%) or prepared fresh from dry powder (Roche Biochemicals), determined to be ∼99.7% pure by HPLC; not shown, see ref *5*). *N*-Methylanthraniloyl-ADP (mantADP) was prepared as described (*9*). ATP and ADP concentrations were determined by absorbance at 259 nm using ϵ_{259} of 15 400 M^{-1} cm^{-1}; mant-ADP concentrations were measured at 255 nm using ϵ_{255} of 23 300 M^{-1} cm^{-1}. A molar equivalent of $MgCl_2$ was added to nucleotides immediately before use.

Actin was purified from rabbit skeletal muscle and gel-filtered (*10*). Platelet actin (85% β:15% γ) was purchased from Cytoskeleton (Denver, CO) and gel filtered. Actin concentrations were determined by absorbance at 290 nm using ϵ_{290} of 2.66×10^4 M^{-1} cm^{-1} (*11*). Pyrene labeling of

† E.M.D.L.C. is a Burroughs Wellcome Fund Fellow of the Life Sciences Research Foundation. This work was supported by the National Institutes of Health Grants GM57247 to E.M.O and AR35661 to H.L.S.

* To whom correspondence should be addressed. Phone: (215) 573-9758. Fax: (215) 573-1171. E-mail: ostap@mail.med.upenn.edu.

[1] Abbreviations: myosin V-1IQ, single-headed myosin V with one light chain binding domain and one bound light chain; CaM, calmodulin; LC, light chain; ELC, essential light chain; trELC, truncated essential light chain; mant-ADP, *N*-methylanthraniloyl-adenosine 5′-diphosphate; V_{max}, maximum steady-state ATPase rate; ATPase, adenosine triphosphatase.

10.1021/bi001701b CCC: $19.00
Published on Web 10/26/2000

Scheme 1

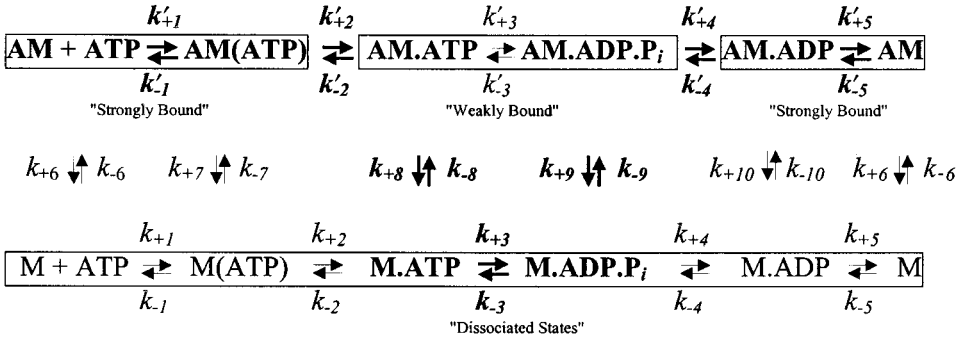

actins was performed as described (*12*). Ca-actin was converted to Mg-actin with 0.2 mM EGTA and 50 μM $MgCl_2$ and polymerized by dialysis (3 × 0.5 L) into KMg50 buffer (50 mM KCl, 1 mM $MgCl_2$, 1 mM EGTA, 1 mM DTT, and 10 mM imidazole, pH 7.0). Phalloidin (Sigma) was used to stabilize actin filaments.

The cDNA for chicken myosin V was truncated at the codon corresponding to amino acid R792, to create a single-headed fragment with the motor domain and one IQ motif (myosin V-1IQ). A flag tag was added to enable purification, as previously described (*2*). A recombinant baculovirus was generated from the myosin V-1IQ construct and coexpressed with baculoviruses encoding either one or a combination of the following essential light chains (ELCs) or calmodulin (CaM): (a) the ELC, LC-1sa (accession no. P14649); (b) truncated LC-1sa; (c) the ELC, LC-17b (accession no. MOCH6N); or (d) CaM (accession no. MCCH). The expressed myosin V-1IQ, with either a bound ELC or CaM, was purified as described (*2*). The truncated essential light chain (trLC-1sa) was produced by deleting the amino acids 2−58 of LC-1sa. Quantitative scanning densitometry of SDS−PAGE gels showed a 1:1 myosin to light chain stoichiometry for all light chain isoforms. The contrast in Figure 1 was digitally adjusted to show clearly both the light chain and heavy chain.

To ensure complete binding of CaM at low protein concentrations, excess (20−40 μM) CaM was included during all measurements with myosin V1IQ CaM.

Steady-State ATPase Activity of 1IQ and Acto1IQ. Steady-state ATPase activities were measured in KMg50 buffer at 25 °C using the NADH-coupled assay as described (*5*).

Stopped-Flow, Quenched-Flow, and Kinetic Modeling. Transient kinetic measurements were made in KMg50 buffer at 25 °C with an Applied Photophysics (Surrey, U.K.) SX.18MV stopped-flow having a 1.2 ms dead time (*2*). Tryptophan fluorescence was measured using a 320 nmWG long-pass emission filter (λ_{ex} = 295 nm). A 400 nm filter was used to monitor pyrene (λ_{ex} = 365 nm), mantADP (λ_{ex} = 295 or 365 nm), and NADH (λ_{ex} = 340 nm) fluorescence. Usually four to seven transients were averaged before nonlinear least-squares fitting. The time courses presented in the figures show raw unaveraged data or the average of two individual traces. Transient P_i release was measured by using the coupled assay system containing the fluorescently labeled mutant of the phosphate-binding protein with the stopped-flow in sequential mixing mode using a 455 nm long-pass filter [λ_{ex} = 430 nm (*2*, *13*)]. The dead time of the instrument in this configuration was 2 ms. Quenched-flow measurements were performed with a KinTek (State College, PA) RQF-3 apparatus (*2*). Errors reported are standard errors in the fits.

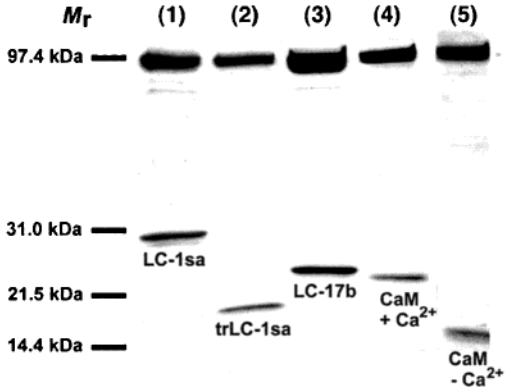

FIGURE 1: Subunit composition of myosin V-1IQ. Coomassie stained SDS−polyacrylamide gel of the myosin V-1IQ heavy chain (upper band; 92.2 kDa) and associated light chain (lower band; 17−23 kDa). Each lane contains the myosin V-1IQ heavy chain and one of four bound light chain isoforms: (1) LC-1sa; (2) truncated LC-1sa; (3) LC-17b (nonmuscle ELC); and (4) CaM. Lane 5 is a different gel of myosin V-1IQ-CaM in the presence of Ca^{2+}. Note the shift in the mobility (4 vs 5) of the CaM, confirming its identity. The other light chains have essentially identical mobilities in the presence and absence of Ca^{2+} (not shown). The subunit stoichiometries are one light chain per heavy chain as determined from scanning densitometry of stained gels.

Kinetic modeling and simulations were performed using the following simplified reaction scheme of the actomyosin V ATPase [Scheme 1 (*2*, *5*)]. The predominant ATPase pathway is shown in bold.

RESULTS

Subunit Composition. If the chicken myosin V-1IQ construct is coexpressed with the two nonmuscle myosin essential light chains isoforms (LC-1sa or LC-17b) and CaM, only LC-1sa binds. When LC-17b and CaM are coexpressed, then only LC-17b binds, but if CaM is coexpressed in the absence of ELC expression, then it binds to the myosin V-1IQ. Thus, either LC-17b or LC-1sa will bind to myosin V-1IQ at a 1:1 stoichiometry with the heavy chain when expressed separately (Figure 1), but only LC-1sa binds if both are available. We find that under no condition will the nonmuscle regulatory light chain bind to myosin V-1IQ (data not shown). While we did not determine binding affinities of any of these subunits for myosin V, the coexpression experiments suggest that the relative order of affinity for the first IQ motif of myosin V is LC-1sa > LC-17b > CaM.

Table 1: Parameters for Nucleotide Binding to Actomyosin V-1IQ Isoforms[a]

	LC-1sa ($\beta\gamma$)[b]	LC-1sa (α)	trLC-1sa (α)	LC-17b (α)	CaM (α)
steady-state					
V_{max} (s^{-1} $head^{-1}$)	16.8 (± 0.8)[c]	17.3 (± 0.8)	15.7 (± 0.6)	19.3 (± 1.5)	14.2 (± 0.5)
K_{ATPase} (μM)	2.1 (± 0.5)	2.5 (± 0.5)	4.1 (± 0.6)	1.0 (± 0.4)	12.7 (± 1.3)
ATP binding					
$K_1'k_2'$ (μM^{-1} s^{-1})	0.75 (± 0.02)	0.90 (± 0.07)[d]	0.90 (± 0.03)	ND[e]	0.80 (± 0.19)
K_1' (μM)	690 (± 105)	815 (± 200)[d]	470 (± 40)	ND	888 (± 146)
k_{+2}' (s^{-1})	889 (± 58)	870 (± 130)[d]	697 (± 19)	ND	668 (± 49)
mantADP release and binding					
k_{+5}' (s^{-1})	15.9 (± 1.2)	14.0 (± 1.4)	12.7 (± 0.4)	19.4 (± 0.5)	12.8 (± 0.9)
k_{-5}' (μM^{-1} s^{-1})	6.6 (± 0.4)	11.8 (± 0.5)	12.0 (± 0.8)	ND	10.0 (± 0.4)
K_5' (μM)	2.4 (± 0.2)	1.1 (± 0.1)	1.1 (± 0.1)	ND	1.3 (± 0.1)

[a] 50 mM KCl, 1 mM $MgCl_2$, 1 mM EGTA, 1 mM DTT, and 10 mM imidazole (pH 7.0), 25 °C. [b] Column headings identify myosin V-1IQ light chain isoform with the actin isoform in parentheses. [c] Uncertainties represent standard errors in the best fits of the data. [d] Values from De La Cruz et al. (1999). [e] ND, not determined.

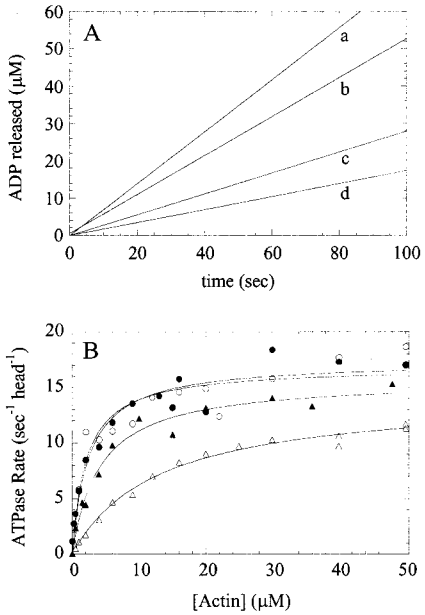

FIGURE 2: Steady-state ATPase of myosin V. (A) Time course of steady-state ATP turnover by 45 nM myosinV-1IQ-LCS1a at (curve a) 16 μM, (curve b) 4 μM, (curve c) 1 μM, and (curve d) 0.5 μM $\beta\gamma$-actin filaments using the NADH-coupled assay. B. Actin filament concentration dependence of the steady-state turnover rate of (○) myosin V-LC-1sa with $\beta\gamma$-actin, (●) myosin V-LC-1sa with α-actin, (▲) myosin V-trLC-1sa with α-actin, and (△) myosin V-CaM with α-actin. The solid lines through the data represent the best fits to a rectangular hyperbola (y = Start + [Amplitude × x)/($K_{0.5}$ + x)]. The steady-state parameters determined from the fit (Start = v_o, Amplitude = V_{max} − v_o, $K_{0.5}$ = K_{ATPase}) are presented in Table 1.

Steady-State ATPase Activity. The steady-state MgATPase activity of myosin V-1IQ is activated by actin filaments (Figure 2). The actin concentration at half-maximum of the steady-state ATPase rate (K_{ATPase}) of myosin V-1IQ LC-1sa is 2.5 (±0.5) μM with rabbit skeletal actin (α-actin) and 2.1 (±0.5) with $\beta\gamma$-actin (Table 1). The maximum ATPase rate (V_{max}) at saturating actin filament concentrations is ∼17 s^{-1} $head^{-1}$ with both actin isoforms (Table 1). Truncating LC-1sa to remove the extended N-terminus (trLC-1sa) which may interact directly with actin (*14*, *15*) does not significantly affect the V_{max} but slightly raises the K_{ATPase} to 4.1 (±0.6) μM (Table 1). The steady-state ATPase parameters of myosin V-1IQ with bound LC-17b are not statistically different from myosin V-1IQ with LC1sa (Table 1). Substituting CaM for an ELC also has no effect on V_{max} but increases the K_{ATPase} ∼6-fold to 12.7 (±1.3) μM. The K_{ATPase}, but not the V_{max}, of myosin V-1IQ-CaM approximates previously reported values under comparable experimental conditions (*3*, *4*).

Table 2: Parameters for Nucleotide Binding to Myosin V-1IQ in the Absence of Actin[a]

parameter	light chain isoform		
	LC-1sa	trLC-1sa	CaM
steady-state			
ATP turnover (s^{-1})[b]	0.02	0.02	0.02
ATP binding and hydrolysis			
K_1k_2 (μM^{-1} s^{-1})	1.4 (± 0.2)	1.6 (± 0.1)	1.3 (± 0.2)
$k_{+3} + k_{-3}$ (s^{-1})[c]	770 (± 16)	567 (± 50)	378 (± 31)
K_3[d]	>10	ND	0.75 (± 0.02)

[a] 50 mM KCl, 1 mM $MgCl_2$, 1 mM EGTA, 1 mM DTT, and 10 mM imidazole (pH 7.0), 25 °C. [b] Single-turnover tryptophan fluorescence measurements, standard errors are ±1 × 10^{-3} for all three isoforms. [c] Tryptophan fluorescence. [d] Quenched-flow.

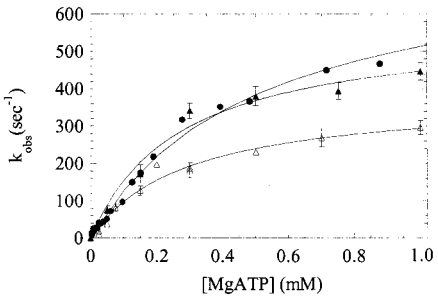

FIGURE 3: MgATP binding to myosin V-1IQ isoforms by tryptophan fluorescence enhancement. Dependence of the rate of (●) myosin V-LC-1sa, (▲) myosin V-trLC-1sa, and (△) myosin V-CaM tryptophan fluorescence enhancement on ATP concentration. Uncertainty bars are standard errors in the fits of the time courses to single exponentials. Solid lines through the data represent the best fits to a rectangular hyperbola. Kinetic and equilibrium parameters are presented in Table 2.

From single turnover measurements, the ATPase rate of all myosin V-1IQ isoforms in the absence of actin filaments is 0.02 s^{-1} (Table 2). Therefore, actin maximally activates the myosin V-1IQ ATPase ∼850-fold, independent of the light chain or actin isoform (Table 1).

MgATP Binding to Myosin V-1IQ Isoforms. We used tryptophan fluorescence enhancement of myosin V-1IQ to measure rates of ATP binding and hydrolysis (*2*) in the absence of actin filaments (Figure 3). At low ATP concentrations the rate of fluorescence enhancement is a direct measure of the rate of ATP binding (*2*). As with other

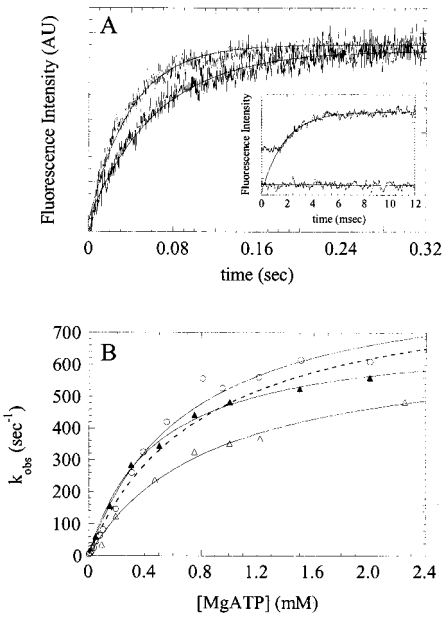

FIGURE 4: MgATP induced population of weakly bound actomyosin V-1IQ states. (A) Time course of fluorescence increase after mixing 40 μM (left) or 20 μM (right) MgATP with 0.5 μM myosin V-LC-1sa bound to pyrene $\beta\gamma$-actin. The inset shows the time course after mixing 2 mM MgATP (curve) or 0 mm MgATP (lower flat trace) with 0.8 μM myosin V-trLC-1sa bound to pyrene α-actin. The solid lines are the best fits to single exponentials [y = Amp $(1 - e^{-kt})$ + Start]. (B) ATP concentration dependence of the k_{obs} for (○) myosin V-LC-1sa with $\beta\gamma$-actin, (▲) myosin V-trLC-1sa with α-actin, and (△) myosin V-CaM with α-actin. Solid lines are the best fits of the data points to a hyperbola. The data points for myosin V-LCS1a with α-actin are left out for clarity; the best fit to the data is represented by the dashed curve.

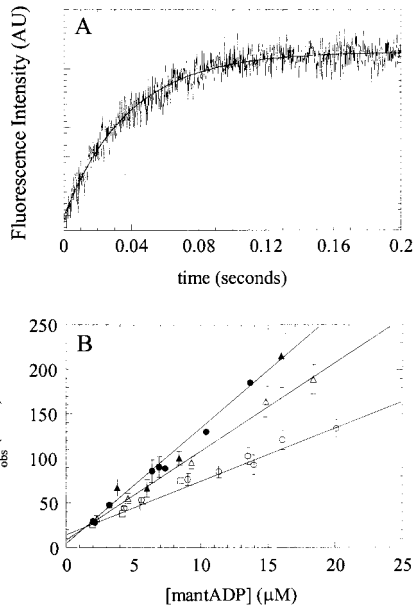

FIGURE 5: Kinetics of mantADP binding to actomyosin V-1IQ. (A) Time course of fluorescence increase after mixing 2.0 μM mantADP with 0.4 μM $\beta\gamma$-actomyosin V 1IQ-LC-1sa. The solid line is the best fit to a single exponential with a rate of 25.8 s^{-1}. B. Dependence of k_{obs} on [mantADP]. Symbols are (○, □) myosin V-LC-1sa with $\beta\gamma$-actin, λ_{ex} = (○) 295 nm or (□) 365 nm; (●) myosin V-LC-1sa with α-actin; (△) myosin V-CaM with α-actin. The data points for myosin V-trLC-1sa with α-actin overlay LC-1sa with α-actin and are not shown for clarity. The rate and equilibrium constants for mantADP binding are presented in Table 1.

myosins (*16*), the maximum rate of the fluorescence enhancement of myosin V 1IQ at high [ATP] presumably reports the rate of ATP hydrolysis ($k_{+3} + k_{-3}$).

Time courses of tryptophan fluorescence enhancement after mixing myosin V-1IQ with ATP follow single-exponential functions at all ATP concentrations examined. The association rate constant for MgATP binding (K_1k_{+2} in Scheme 1) determined from the initial slope is 1.3−1.6 μM^{-1} s^{-1} with all myosin V-1IQ light chain isoforms (Table 2). Therefore, light chain isoform differences do not significantly affect the rate of ATP binding. However, there is a significant reduction in the maximum rate ($k_{+3} + k_{-3}$) as determined by fitting the data to a hyperbola when trLC-1sa or CaM are bound (Table 2). The maximum rate is highly temperature dependent (47 s^{-1} at 8 °C vs 770 s^{-1} at 25 °C for myosin V-1IQ-LC-1sa), consistent with this transition monitoring the conformational change that precedes and limits ATP hydrolysis (*2*).

ATP−Induced Population of the Weakly-Bound States. Pyrene fluorescence was used to monitor the ATP-induced population of the weakly bound myosin states. Actomyosin concentrations lower than the K_{ATPase} (Table 1) were used to ensure ATP-induced dissociation of myosin V-1IQ from actin. Time courses of the fluorescence increase after mixing pyrene actomyosinV-1IQ with ATP follow single exponentials (Figure 4A) with rates that depend hyperbolically on the MgATP concentration (Figure 4B). The pyrene-actin fluorescence in the presence of ATP for all myosin V-1IQ light chain isoforms was within 10% of the fluorescence of pyrene-actin alone, indicating the loss of the AM and AM-(ATP) states (Scheme 1). The maximum rate of the fluorescence change (k'_{+2}) is independent of the actin isoform (Table 1), but is reduced when CaM or trLC-1sa are bound (Table 1). The rate constant for ATP binding obtained from the initial slope ($K'_1k'_{+2}$) is between 0.75 and 0.90 μM^{-1} s^{-1} with all light chain and actin isoforms (Table 1). The ATP concentration dependence of k_{obs} deviates from the best fit to a hyperbola with $\beta\gamma$-actin (Figure 4B), perhaps reflecting some form of cooperativity within the actin filament specific to $\beta\gamma$-actin.

ADP Binding and Dissociation by mantADP and Tryptophan Fluorescence. Time courses of fluorescence enhancements after mixing mantADP with actomyosin V-1IQ follow single exponentials (Figure 5A) for each light chain and actin isoform with rates that depend linearly on the concentration of nucleotide (Figure 5B). The apparent second-order rate constants (k'_{-5}) obtained from the slopes of the lines depend on the actin and light chain isoform (Table 1). The value for mantADP binding to α-actomyosin V-1IQ with bound LC-1sa is 11.8 (±0.5) μM^{-1} s^{-1} and agrees with earlier determinations (*2*). The rate is reduced approximately 2-fold [k'_{-5} = 6.6 (±0.4) μM^{-1} s^{-1}] with $\beta\gamma$-actin and to a lesser extent [k'_{-5} = 10.0 (±0.4) μM^{-1} s^{-1}] when CaM is the bound light chain. Truncating LC-1sa to remove the actin-binding extension does not affect the mantADP-binding rate (Table 1).

The rates of mantADP dissociation (k'_{+5}) from all actomyosin V-1IQ isoforms approximate the actin-activated steady-state ATPase rates (Table 1), consistent with ADP release being rate-limiting in the actomyosin V ATPase cycle (*2*).

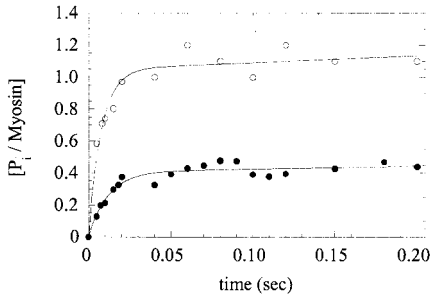

FIGURE 6: P_i burst of myosin V-1IQ CaM. Time course of ADP−P_i formation by (●) myosin V 1IQ-CaM (3.0 μM with 2-fold molar excess of CaM) or (○) myosin V 1IQ-LC-1sa (3.2 μM) after mixing with 100 μM ATP. The solid lines are the best fits of the data to single exponentials with a rate of 84 (±13) s^{-1} and an amplitude (Burst) of 0.43 (±0.03) P_i/myosin head for 1IQ-CaM; the rate is 120 (±20) s^{-1} and burst is 1.05 (±0.06) P_i/myosin for 1IQ with bound LC-1sa. The data for LC-1sa is taken from ref *3*.

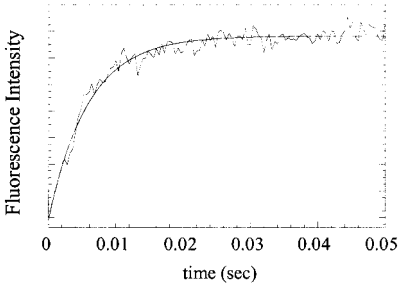

FIGURE 7: Rate of P_i release from actomyosin V-1IQ CaM. Myosin V 1IQ-CaM (3.0 μM with 20 μM free CaM) was mixed with 1 mM MgATP, aged for 14 ms to populate the weak-binding states, then rapidly mixed with a solution of actin filaments and P_i-binding protein. Final concentrations at $t = 0$ were 0.8 μM 1IQ-CaM, 250 μM MgATP, 6 μM P_i-binding protein and 30 μM α-actin filaments. The solid line is the best fit to an exponential with a rate of 176 (±9) s^{-1}. The dead time was 2 ms.

ADP binding does not change the myosin V-1IQ tryptophan fluorescence (data not shown, ref *3*), so we measured ADP dissociation (k_{+5}) from the fluorescence enhancement after mixing an excess of ATP with myosin V-1IQ-ADP (with LC-1sa bound). We obtained k_{+5} of 1.8 s^{-1} which ∼1.5 times more rapid than the value obtained with mantADP (k_{+5} = 1.2 s^{-1}; ref *2*), demonstrating that fluorescent modification of the nucleotide does not dramatically affect the rate of dissociation from myosin V-1IQ. In the presence of actin, the effect is even less significant (*2*).

The ADP affinities (K'_5) calculated from the ratio of rate constants (k'_{+5}/k'_{-5}) are ∼1 μM for myosin V-1IQ bound to α-actin regardless of the light chain isoform (Table 1). The ADP affinity is 2-fold lower in the presence of $\beta\gamma$-actin (Table 1) due to a slower association rate constant.

ATP Hydrolysis and P_i Burst. We measured the P_i burst of myosin V-1IQ with bound CaM by quench flow (Figure 6). The amplitude of the phosphate burst is 0.43 (±0.01) P_i/myosin. Assuming $k_{+2} \gg k_{-2}$ (Figure 3) and k_{+4} is rate limiting in the absence of actin (*2*), the burst (*B*) is related to the equilibrium constant for ATP hydrolysis (K_3) by $B = K_3/(1 + K_3)$, where $K_3 = (k_{+3}/k_{-3})$ (*16*, *17*). This yields a value of $K_3 = 0.75$ (±0.02). This is significantly lower than the K_3 obtained for myosin V-1IQ with bound LC-1sa ($K_3 > 10$; Figure 6; ref *2*).

Transient P_i Release. We directly measured the rate (k'_{+4}; Scheme 1) of P_i release from M·ADP·P_i after mixing with 30 μM α-actin filaments (Figure 7). The time course of phosphate release by myosin V-1IQ CaM follows a single exponential with a rate of 176 (±9) s^{-1}, which is comparable to myosin V-1IQ with bound LC-1sa (*2*). As shown previously (*2*), the rate of P_i release depends linearly on actin concentrations <40 μM and occurs at a maximum rate >250 s^{-1}. Therefore, P_i release from myosin V-1IQ with bound CaM is (a) limited by the rate of M·ADP·P_i binding to actin ($k_{-9} = 5-6$ μM^{-1} s^{-1}; Scheme 1) at <40 μM actin, and (b) *is not* rate limiting for myosin V. ADP release is the rate-limiting step in the cycle (refs *2* and *5*; Table 1).

DISCUSSION

The actin isoform has little effect on most of the measured kinetic parameters of myosin V-1IQ. The apparent second-order rate constant for ADP binding (k'_{-5}) is ∼2-fold slower with $\beta\gamma$-actin (Table 1). Therefore, the use of skeletal muscle α-actin does not alter the values or interpretation of myosin V kinetic parameters (*2*−*4*). However, we cannot exclude a role for actin-binding proteins in modulating the in vivo kinetics of myosin V.

The rationale for comparing the two essential light chain (ELC) isoforms, is that both of these isoforms are expressed in mammalian cells, as are the nonmuscle regulatory light chain (RLC) and CaM (*18*). Thus all of these light chains are available for potential binding to myosin V. The IQ motif adjacent to the motor domain is capable of binding either of two ELC isoforms or CaM (Figure 1). On the basis of our coexpression studies, we propose that myosin V has an ELC bound to the first IQ motif. Given that the nonmuscle ELC, LC-17b, is expressed in most tissues, and that LC-1sa is absent in many adult tissues and perhaps in some species (*18*), LC-17b is likely associated with the first IQ in most adult vertebrates. Because both LC-1sa and LC-17b gave identical steady-state V_{max} and K_{ATPase} values (Table 1), the rate constants that define the duty ratio are most likely the same (see below). Therefore, we confined our detailed investigation to myosin V-1IQ LC-1sa. In addition, our preparations yielded sufficient quantities of protein for a detailed kinetic characterization, whereas, myosin V-1IQ with LC-17b did not.

Most kinetic parameters of myosin V-1IQ are not affected by the identity of the light chain occupying the IQ motif adjacent to the motor domain. The V_{max} of the steady-state ATPase, the actin-activated rate of P_i release (k'_{+4}), the rates of ADP binding (k'_{-5}) and dissociation (k'_{+5}), and the ADP equilibrium binding affinity (K'_5) for the actomyosin V-1IQ complex are all indistinguishable, within experimental error. This confirms that the myosin V-1IQ actin-activated ATPase cycle is limited by ADP release (*2*), regardless of the actin or light chain/calmodulin isoform (in the absence of calcium).

There are three notable kinetic alterations when CaM occupies the IQ motif adjacent to the motor domain: (a) a >2-fold reduction in the amplitude of the phosphate burst (Figure 6); (b) a 2-fold reduction in the maximum rate of intrinsic tryptophan fluorescence enhancement (Figure 3), which likely reports the structural change that limits the rate of ATP hydrolysis ($k_{+3} + k_{-3}$); and (c) an increase in the

K_{ATPase} of the actin-activated steady-state activity (Figure 2, Table 1). The maximum rate of tryptophan fluorescence change and the K_{ATPase} are in reasonable agreement (given the different temperatures) with those reported for mouse myosin V with bound CaM (*3*, *4*) and suggests that the kinetic behavior of myosin V isoforms (*2*−*4*) are influenced primarily by the light chain, rather than the heavy chain isoform (mouse vs chicken).

The decreased myosin V-1IQ CaM phosphate-burst can result from (a) a decrease in the equilibrium constant for ATP hydrolysis (K_3), (b) an increase the number of inactive myosin molecules, (c) an increase in the rate of ATP dissociation (k_{-2}), or (d) ADP contamination. Single turnover (Table 2) and steady-state hydrolysis (Figure 2) measurements confirm that the mole fraction of active myosin V-1IQ CaM is >0.95. In addition, myosin V-1IQ CaM dissociates almost completely from 0.5 μM pyrene-actin as determined by fluorescence measurements in the presence of ATP, thus showing (a) that >95% of the myosin is capable of binding ATP, and (b) that ATP binding is irreversible (i.e., $k'_{+2} \gg k'_{-2}$) in the presence of actin. Although we have not directly measured k_{-2} for myosin V-1IQ CaM, it is unlikely to be large enough (>500 s^{-1}) to account for the >2-fold decrease in the phosphate burst. Finally, contaminating ADP is removed from protein solutions prior to all experiments by exhaustive dialysis and apyrase treatments as described (*2*, *5*). This treatment successfully removes contaminating ADP from myosin V-1IQ LC-1sa (*2*, *5*) which has a similar ADP affinity as myosin V-1IQ CaM (Table 1), and is thus expected to decontaminate myosin V 1-IQ CaM. Therefore, the decrease in the phosphate burst for myosin V-1IQ CaM is most likely due to a decrease in K_3.

The low K_{ATPase} of myosin V with bound LC-1sa does not result from the actin-binding properties of LC-1sa. Although the lysine-rich 58 amino acid N-terminal extension may bind actin filaments directly (*14*, *15*), its removal (truncated LC-1sa) alters the K_{ATPase} by less than a factor of 2 (Table 2) and shows a modest reduction in the rate of ATP hydrolysis ($k_{+3} + k_{-3}$; Table 2). Therefore, light-chain-dependent changes in the K_{ATPase} are most likely due to modulation of the ATPase kinetics by direct interactions of the light chain with the myosin V motor domain. Additional support for this conclusion is that when LC-17b, which lacks an N-terminal extension, is bound, the myosin V 1IQ has a K_{ATPase} that is similar to that of the LC-1sa containing construct.

We can attribute the light-chain-isoform dependent K_{ATPase} values to differences in the equilibrium constant for ATP hydrolysis (K_3). Using a simplified steady-state ATPase reaction scheme (Scheme 2):

Scheme 2

$$M{\cdot}ATP \overset{K_3^{app}}{\rightleftharpoons} M{\cdot}ADP{\cdot}P_i \xrightarrow{k_{-9}} AM{\cdot}ADP + P_i \xrightarrow{k'_{+5}} AM + ADP$$

where M·ATP and M·ADP·P_i are in equilibrium, P_i release (k'_{+4}; Scheme 1) is limited by the rate of actin binding to the M·ADP·P_i intermediate (k_{-9}) at actin concentrations <40 μM (*2*), k_{+9} and k'_{-5} are small compared to corresponding forward reactions (*2*), then the K_{ATPase} is the same as the apparent dissociation constant for the AM·ADP:

$$K_{ATPase} = \frac{[\text{non-AM}{\cdot}\text{ADP states}]}{[\text{AM}{\cdot}\text{ADP}]} = \frac{\text{rate of AM}{\cdot}\text{ADP loss}}{\text{rate of AM}{\cdot}\text{ADP formation}} \quad (1)$$

Therefore, the K_{ATPase} can be related to K_3^{app} according to

$$K_{ATPase} = \frac{k'_{+5}}{k_{-9}\left(\frac{K_3^{app}}{1 + K_3^{app}}\right)} \quad (2)$$

$K'_1k'_{+2}$, k'_{-2}, k'_{+5}, and k_{-9} are nearly identical for all of the light chain constructs (Table 1), so the differences in the K_{ATPase} must be due to changes in K_3^{app}. Using eq 2, we calculate the K_3^{app} to be ~0.4 for myosin V-1IQ with bound CaM and ~8 for myosin V-1IQ with bound LC-1sa. These calculated values for K_3^{app} are within a factor of 2 of the experimentally determined values for K_3 in the absence of actin (Figure 6, Table 2) (*2*).

Using the experimentally determined equilibrium constants for ATP hydrolysis (K_3; Table 2) and the maximum rates of tryptophan fluorescence ($k_{+3} + k_{-3}$; Table 2), the forward and reverse rates of ATP hydrolysis can be calculated as $k_{+3} > 700$ s^{-1} and $k_{-3} < 70$ s^{-1} for myosin V-1IQ with LC-1sa and $k_{+3} = 162$ s^{-1} and $k_{-3} = 216$ s^{-1} for myosin V-1IQ with CaM. This >4-fold reduction in k_{+3} and >3-fold increase in k_{-3} shows that myosin-V IQ with LC-1sa significantly favors the M·ADP·Pi state. It is possible that CaM makes different contacts with the motor than does an ELC (*19*).

One implication of a reduced K_3 is that occupancy of the AM·ADP states will decrease in the steady state, which will reduce the duty ratio (fraction of myosin heads strongly bound to actin). Since the AM state [Scheme 1 (2)] is not significantly populated during steady-state ATP hydrolysis, the duty ratio of a steady-state population of single-headed myosin V-1IQ is defined as the mole fraction of the AM·ADP state:

$$\text{duty ratio} = \frac{[\text{AM}{\cdot}\text{ADP}]}{[\text{all myosin states}]} = \frac{(\text{rate of AM}{\cdot}\text{ADP formation})}{(\text{rate of AM}{\cdot}\text{ADP formation}) + (\text{rate of AM}{\cdot}\text{ADP loss})} \quad (3)$$

Therefore, the duty ratio as a function of actin concentration can be calculated using Scheme 2 as

$$\text{duty ratio} = \frac{[A]k_{-9}\left(\frac{K_3^{app}}{1 + K_3^{app}}\right)}{[A]k_{-9}\left(\frac{K_3^{app}}{1 + K_3^{app}}\right) + k'_{+5}} \quad (4)$$

where [A] is the actin filament concentration. The calculated duty ratios (Figure 8) clearly show that myosin V-1IQ with bound LC-1sa has a higher duty ratio than myosin V-1IQ with bound CaM at low actin concentrations and 25 °C. Also

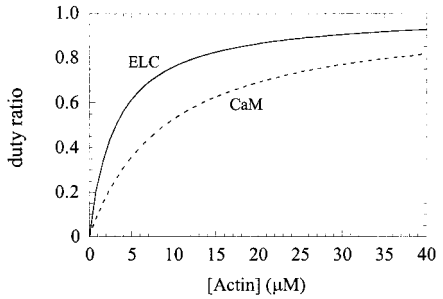

FIGURE 8: Actin concentration dependence of the duty ratio of single headed myosin V. The duty ratio of myosin V 1IQ with bound LC-1sa (solid curve) or CaM (dashed curve) was calculated with eq 2 using the corresponding ADP release rates (k'_{+5}; Table 2), $k_{-9} = 5\ \mu M^{-1}\ s^{-1}$ for both isoforms, $K_3 = 0.4$ for myosin V-1IQ with CaM, and $K_3 = 8$ myosin V-1IQ with LC-1sa.

note that since ADP release is rate limiting and P_i release is fast, the predominant steady-state intermediates (AM·ADP) are strongly bound to actin, so the actin concentration yielding half of the maximum steady-state ATPase rate (K_{ATPase}; Figure 2, Table 1) must be the same as the actin concentration that generates 50% strongly bound heads (K_{dr}; Figure 8; i.e., $K_{ATPase} = K_{dr}$).

The kinetic differences among the light chain isoforms are probably not significant under cellular conditions. This is primarily due to the fact that for other characterized myosins, increasing the temperature to 37 °C shifts the equilibrium constant for ATP hydrolysis (K_3) toward the M·ADP·P_i state (*20*). At 37 °C, the phosphate burst ($K_3/1 + K_3$) is expected to approach one, and thus the duty ratio (eq 4) will depend only on the light-chain independent rate constants k_{-9} and k'_{+5} (eq 4; Table 1). Therefore at physiological temperatures, the identity of the light chain is unlikely to alter the degree of myosin V processivity. We found that the K_{ATPase} of myosin V-1IQ CaM drops to 2.8 (±0.4) μM at 37 °C (data not shown), which is supported by Trybus et al. (1999; ref *3*) who found the K_{ATPase} of mouse myosin V-1IQ CaM decreases ~20-fold to ~1.0 μM as the temperature is increased from 25 to 37 °C. Of important technical note for single molecule studies of processivity (*1*), is that at 25 °C and in the absence of ADP, the duty ratio will be significantly reduced by CaM binding to the first IQ motif of myosin V.

ACKNOWLEDGMENT

We thank Dan Safer, Corry Baldacchino, and Zhaohui Yang for technical assistance. We thank Steven S. Rosenfeld (University of Alabama) for phosphate binding protein and mant-ADP.

REFERENCES

1. Mehta, A. D., Rock, R. S., Rief, M., Spudich, J. A., Mooseker, M. S., and Cheney, R. E. (1999) *Nature 400*, 590−593.
2. De La Cruz, E. M., Wells, A. L., Rosenfeld, S. S., Ostap, E. M., and Sweeney, H. L. (1999) *Proc. Natl. Acad. Sci. U.S.A. 96*, 13726−13731.
3. Trybus. K. M., Krementsova, E., and Freyzon, Y. (1999) *J. Biol. Chem. 274*, 27448−27456.
4. Wang, F., Chen, L., Arcucci, O., Harvey, E. V., Bowers, B., Xu, Y., Hammer, J. A., III, and Sellers, J. R. (2000) *J. Biol. Chem. 275*, 4329−4335.
5. De La Cruz, E. M., Sweeney, H. L., and Ostap, E. M. (2000) *Biophys J. 79*, 1524−1529.
6. Houdusse A, Silver, M. and Cohen, C. (1996) *Structure 4*, 1475−90.
7. Houdusse., A, Kalabokis, V. N., Himmel, D., Szent-Gyorgyi, A. G., and Cohen, C. (1999) *Cell 97*, 459−470.
8. Cheney, R. E., O'Shae, M. K., Heuser, J. E., Coelho, M. V., Wolenski, J. S., Espreafico, E. M., Forscher, P., Larson, R. E., and Mooseker, M. S. (1993) *Cell 75*, 13−23.
9. Hiratsuka, T. (1983) *Biochim. Biophys. Acta 742*, 496−508.
10. MacLean-Fletcher, S., and Pollard, T. D. (1980) *Bioch. Biophys. Res. Comm. 96*, 18−27.
11. Houk, T. W., Jr., and Ue, K. (1974) *Anal. Biochem. 62*, 66−74.
12. Pollard, T. D. (1984) *J. Cell Biol. 99*, 769−777.
13. White H. D., Belknap B., and Webb, M. R. (1997) *Biochemistry 36*, 11828−11836.
14. Sutoh, K. (1982) *Biochemistry 21*, 3654−3661.
15. Milligan, R. A., M. Whittaker, and D. Safer (1990) *Nature 348*, 217−221.
16. Johnson, K. A., and Taylor, E. W. (1978) *Biochemistry 17*, 3432−3442.
17. Taylor, E. W. (1977) *Biochemistry 16, 732−739.*
18. Hailstones, D. L. and Gunning, P. W. (1990) *Mol. Cell. Biol. 10*, 1095−1104.
19. Rayment, I., Rypniewski, W. R., Schimdt-Base, K., Smith, R., Tomchick, D. R., Benning, M. M., Winkelman, D. A., Wesenberg, G., and Holden, H. M. (1993) *Science 261*, 50−58.
20. Kodama, T. (1985) *Physiol. Rev. 65*, 467−551.

BI001701B